

# GALACTIC CHEMICAL EVOLUTION: THE IMPACT OF THE $^{13}\text{C}$ -POCKET STRUCTURE ON THE S-PROCESS DISTRIBUTION

S. Bisterzo<sup>1</sup> and C. Travaglio<sup>2</sup>

INAF - Astrophysical Observatory Turin, Turin, Italy

bisterzo@to.infn.it; sarabisterzo@gmail.com

M. Wiescher

Joint Institute for Nuclear Astrophysics (JINA), Department of Physics, University of  
Notre Dame, IN, USA

F. Käppeler

Karlsruhe Institute of Technology, Campus Nord, Institut für Kernphysik, Karlsruhe,  
Germany

and

R. Gallino<sup>2</sup>

Department of Physics, University of Turin, Italy

Received \_\_\_\_\_; accepted \_\_\_\_\_

---

<sup>1</sup>Department of Physics, University of Turin, Italy

<sup>2</sup>B2FH Association-c/o Strada Osservatorio 20, 10023 Turin, Italy

## ABSTRACT

The solar  $s$ -process abundances have been analyzed in the framework of a Galactic Chemical Evolution (GCE) model. The aim of this work is to implement the study by Bisterzo et al. (2014), who investigated the effect of one of the major uncertainties of asymptotic giant branch (AGB) yields, the internal structure of the  $^{13}\text{C}$  pocket. We present GCE predictions of  $s$ -process elements computed with additional tests in the light of the suggestions provided in recent publications. The analysis is extended to different metallicities, by comparing GCE results and updated spectroscopic observations of unevolved field stars. We verify that the GCE predictions obtained with different tests may represent, on average, the evolution of selected neutron-capture elements in the Galaxy. The impact of an additional weak  $s$ -process contribution from fast-rotating massive stars is also explored.

*Subject headings:* Stars: AGB - Galaxy: evolution, abundances

## 1. GCE Solar s-process Predictions

AGB stars with low initial mass are the major responsible for the nucleosynthesis of solar  $s$  isotopes with  $A > 90$  (Busso, Gallino & Wasserburg 1999).

The main neutron source of low-mass AGB models is the  $^{13}\text{C}(\alpha, n)^{16}\text{O}$  reaction, which burns radiatively during the interpulse in a thin layer of the He intershell, the so-called  $^{13}\text{C}$  pocket (Straniero et al. 1995). The formation of the  $^{13}\text{C}$  pocket requires an unknown mixing mechanism that allows partial mixing of a few protons from the convective envelope into the top layers of the radiative He- and C-rich intershell. This is assumed to occur at the quenching of a Third Dredge Up (TDU) episode. When the star contracts, the H shell reignites and protons in the intershell are captured by the abundant  $^{12}\text{C}$  nuclei to yield primary  $^{13}\text{C}$ . If more protons than  $^{12}\text{C}$  nuclei are diffused in the outer layers, a region of primary  $^{14}\text{N}$  may form by further proton captures on  $^{13}\text{C}$ . Subsequently, the temperature in the  $^{12}\text{C}$  pocket increases to  $\sim 1 \times 10^8$  K, and neutrons are released radiatively within the pocket via  $^{13}\text{C}(\alpha, n)$  reactions at quite low neutron densities.

Various physical mechanisms have been explored for the formation of  $^{13}\text{C}$  pocket (e.g., overshooting, rotation, magnetic fields, gravity waves; Herwig et al. 1997; Langer et al. 1999; Denissenkov & Tout 2003; Siess, Goriely, & Langer 2004; Straniero, Gallino & Cristallo 2006; Piersanti, Cristallo, & Straniero 2013; Nucci & Busso 2014). The details of how the  $^{13}\text{C}$  pocket forms are still debated, making its mass extent and the H profile largely uncertain.

Spectroscopic observations provide key information to constrain theoretical models: chemically peculiar  $s$ -rich stars have evidenced a dispersion of the  $s$  abundances for a given metallicity (e.g., MS, S, C(N), Ba, CEMP-s and post-AGB stars, planetary nebulae; see the recent review by Käppeler et al. 2011 and Karakas & Lattanzio 2014). This dispersion has been recognized since first studies by Busso et al. (2001) and Abia et al. (2002), but

the reason(s) are not definitely identified. A variation in the stellar rotational velocity may be regarded as a possible explanation (see Piersanti, Cristallo, & Straniero 2013, and references therein).

Owing to the present uncertainties, the  $^{13}\text{C}$  pocket is artificially introduced in our post-process AGB models, following the observational constraints. The shape of the  $^{13}\text{C}$  and  $^{14}\text{N}$  profiles and the mass involved in the pocket are regulated by a free parametrization. The internal structure of the  $^{13}\text{C}$  pocket adopted so far has been calibrated to represent the solar main component (Arlandini et al. 1999): it is a three-zone pocket (each zone has defined  $X(^{13}\text{C})$  and  $X(^{14}\text{N})$  abundances) with a total mass of about  $0.001 M_{\odot}$  (see Table 1; first group of data). A range of  $^{13}\text{C}$ -pocket strengths is assumed to reproduce the spectroscopic *s*-process dispersion: we parametrically vary the concentration of  $^{13}\text{C}$  (and  $^{14}\text{N}$ ) of each zone given in Table 1 by different factors, leaving the mass of the pocket constant. We refer to Bisterzo et al. (2010, 2014) for a detailed discussion. This systematic approach appears justified by the present uncertainties: the formation of diverse  $^{13}\text{C}$  pockets may result from the interplay between different physical processes in stellar interiors. Post-process models should be considered useful tests to address full stellar evolutionary models (and in general multidimensional/hydrodynamical simulations) against observational constraints.

The solar *s*-process abundances must account for the complex chemical evolution of the Galaxy, which includes AGB yields of various masses and metallicities. The chemical evolution model adopted to reproduce the solar *s* distribution has been exhaustively described by Travaglio et al. (1999, 2004).

In the framework of GCE, we showed that the solar *s* distribution of isotopes with  $130 < A \leq 208$  can be accurately reproduced once we consider a proper weighted average among

the  $^{13}\text{C}$ -pocket strengths<sup>1</sup>. This is consistent with the observed spectroscopic *s*-process dispersion. A deficit (of about 25%) between GCE predictions of *s*-process elements and the solar abundances was found for isotopes with  $90 < A < 130$  (solar LEPP-s). Bisterzo et al. (2014) have investigated a possible connection between this deficit and the  $^{13}\text{C}$ -pocket structure. On the basis of their tests, solar GCE predictions of *s*-process elements are marginally affected.

The aim of this work is to implement the analysis carried out on the  $^{13}\text{C}$ -pocket structure by Bisterzo et al. (2014), (Section 2). In Section 3, we consider the sensitivity of AGB yields to metallicity, focusing on the contribution by metal-rich AGB stars to the light elements (see discussion by Maiorca et al. 2012 for open clusters). Although the solar composition is fundamental to constrain AGB yields, it only provides a single piece of information about the Galactic history. The reliability of the  $^{13}\text{C}$ -pocket tests needs to be verified by considering the complex framework of Galactic chemical enrichment. The GCE predictions of selected neutron-capture elements versus metallicity are compared with updated spectroscopic observations in Section 4. Recently, rotation-induced mixing in low-metallicity massive stars has been proposed as an explanation of the observed [Sr/Ba] dispersion in extremely metal-poor stars, being efficient primary producers for *s* isotopes heavier than Sr, up to the Ba neutron-magic peak (Frischknecht, Hirschi, & Thielemann 2012; Pignatari et al. 2013; Cescutti et al. 2013). In this context, we investigate the impact of recent weak *s*-process yields by Frischknecht et al. (2016), available from a large grid

---

<sup>1</sup>To this purpose, the unbranched *s*-only isotope  $^{150}\text{Sm}$  is taken as reference nuclide for the whole *s*-process distribution. The high production of  $^{208}\text{Pb}$  in low-mass low-metallicity AGB stars plays another indicative GCE constraint (Travaglio et al. 2001). The solar abundance of  $^{208}\text{Pb}$  is matched once the *s*-process occurring in low-metallicity AGB stars is properly considered in the context of the chemical evolution of the Galaxy.

of rotating massive stars ( $Z$  from  $10^{-5}$  to solar), on the Galactic chemical enrichment (Section 4.1).

In Section 5 our results are briefly summarized and future outlook are discussed.

## 2. Impact of New $^{13}\text{C}$ -pocket Tests on Solar $s$ Abundances

We focus on specific additional tests carried out on the basis of recent advice available in literature. The internal  $^{13}\text{C}$ -pocket structure adopted in each test is given in Table 1<sup>2</sup>.

- Starting from the three-zone  $^{13}\text{C}$ -profile adopted so far, we investigate the impact of a substantially extended  $^{13}\text{C}$ -pocket mass than assumed in our previous computations (up to four times larger, corresponding to a total mass of  $M_{\text{tot}}(\text{pocket}) \sim 4 \times 10^{-3} M_{\odot}$ ; see tests described as **CASE 1** and **CASE 2** in Table 1).

In this regard, Maiorca et al. (2012) have proposed such a  $^{13}\text{C}$ -pocket mass to represent the abundances of neutron-capture elements in young open clusters. Magnetic buoyancy (or other forced mechanisms) are suggested as good candidates to form such a  $^{13}\text{C}$  reservoir (Trippella et al. 2014). Rotation models by Piersanti, Cristallo, & Straniero (2013) indicate that low-metallicity AGB stars and fast-rotating metal-rich stars might produce such an extended  $^{13}\text{C}$  pocket. Comparison between theoretical models and the strontium and barium isotopic signatures measured in mainstream SiC grains require  $^{13}\text{C}$  pockets with  $M_{\text{tot}}(\text{pocket}) \geq 1 \times 10^{-3} M_{\odot}$  (Liu et al. 2015).

---

<sup>2</sup>We remind that all tests are performed on low-mass AGB models because the effect of the  $^{13}\text{C}$  pocket in AGB stars with intermediate mass ( $4 \leq M/M_{\odot} < 8$ ) is negligible for GCE solar predictions (see Section 2 by Bisterzo et al. 2014; Straniero, Cristallo & Piersanti 2014).

- In **CASE 3** (see Table 1), we test the effect of an additional parametrized  $^{14}\text{N}$ -pocket. As anticipated in Section 1, an outer  $^{14}\text{N}$ -rich layer may form in the pocket once enough protons are mixed in the external zone of the He intershell (Goriely & Mowlavi 2000; Cristallo et al. 2009, 2011; Karakas et al. 2010; Lugaro et al. 2012; Trippella et al. 2014). The presence of rotation may widen the  $^{14}\text{N}$  pocket by inducing partial mixing of the  $^{14}\text{N}$ -rich region with the inner  $^{13}\text{C}$ -rich zone.

- In **CASE 4**, we have performed a set of 1.5, 2 and 3  $M_{\odot}$  models computed with a more efficient Reimers mass loss than in previous models. This implies that AGB models experience about half of the TDU episodes compared to CASE 3. The  $^{13}\text{C}$  pocket structure is the same as adopted in CASE 3 (see Table 1).

This test simulates the recent prescriptions of updated FRUITY<sup>3</sup> models by Cristallo et al. (2009, 2011). FRUITY models include an efficient AGB mass-loss rate, which has been calibrated using the infrared luminosity function of Galactic carbon stars, and improved radiative C-enhanced opacity tables. Accordingly, these new models with a reduced number of TDU episodes are in better agreement with observations (Guandalini & Cristallo 2013 and references therein).

- Finally, in **CASE 5** (see Table 1), we test the impact of an additional extended inner zone of the pocket with a mass of  $2 \times 10^{-3} M_{\odot}$  and a correspondingly lower  $^{13}\text{C}$  abundance ( $X(^{13}\text{C})=2.75\text{E}-3$ ).

Recently, Cristallo et al. (2015) found that a different convective/radiative boundary condition allows a deeper penetration of protons with a very low mixing efficiency during TDU episodes. The resulting  $^{13}\text{C}$  pocket displays an extended tail with a smooth decrease of the  $^{13}\text{C}$  profile (see *Tail* model in their Fig. 7). CASE 5 roughly approximates the *Tail* model by Cristallo et al. (2015).

---

<sup>3</sup>web: [fruity.oa-teramo.inaf.it/](http://fruity.oa-teramo.inaf.it/).

The resulting solar GCE predictions of  $s$ -process elements are displayed in Fig. 1. A proper weighted average among the various  $^{13}\text{C}$ -pocket strengths must be adopted for each test to reconcile GCE predictions with 100% of solar  $^{150}\text{Sm}$  (see Bisterzo et al. 2014). This approach allows us to reproduce the solar  $^{150}\text{Sm}$  within 5% uncertainty (Lodders, Palme & Gail 2009).

The  $s$ -only isotopes with atomic mass  $A \gtrsim 90$  show variations smaller than  $\sim 10\%$ , thus confirming the need of a solar LEPP- $s$  mechanism in order to increase the solar  $s$  abundances in the range  $90 < A < 130$ , as predicted by Travaglio et al. (2004).

Note that AGB yields computed with a single  $^{13}\text{C}$ -pocket choice do not provide accurate interpretations neither of solar  $s$  abundances nor of observations of peculiar  $s$ -rich stars. By working in a larger range of uncertainties, potential missing contributions are not necessarily highlighted. Accordingly, the result of this paper does not disagree with a recent study by Cristallo et al. (2015) that provides a meticulous discussion about the uncertainties affecting stellar models and the solar GCE distribution. Within the estimated uncertainties a LEPP mechanism is not necessarily required. However, the authors suggest how their representation of the solar distribution could be improved once models with different initial rotational velocities (or different prescriptions for convective overshoot during the TDU) will be included in GCE computations for an extended metallicity grid. These upcoming progresses in stellar models will assess whether additional contributions are needed.

### 3. The Stellar Yields versus Metallicity

The complex dependence of  $s$ -process yields on the initial stellar metallicity is well known. In Fig. 2 (top panel), we display the AGB production factors of selected  $s$ -only isotopes. Starting from  $[\text{Fe}/\text{H}] = -0.5$ , which corresponds to  $t_{\text{Gal}} = 3.5$  Gyr, the  $s$





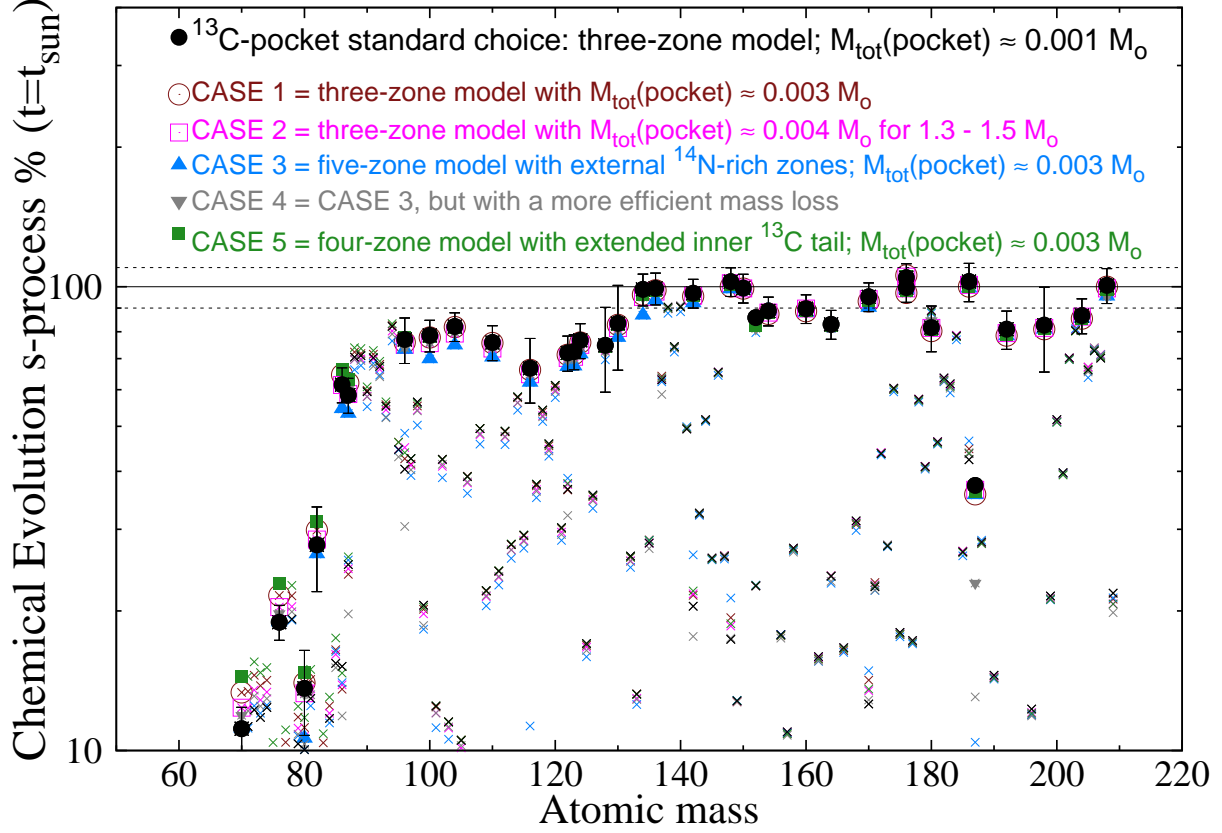


Fig. 1.— Effect of the <sup>13</sup>C-pocket uncertainties in low mass AGB models on GCE solar *s*-process predictions. The *s*-only isotopes (and <sup>208</sup>Pb) obtained with our standard three-zone <sup>13</sup>C-pocket choice are represented by filled circles. Stable nuclei are displayed by crosses. The results obtained by several tests have been displayed with different symbols (see label in the top panel of the figure). We have adopted a range of <sup>13</sup>C-pocket strengths (Table 1) in order to reproduce 100% of solar <sup>150</sup>Sm when changing the structure of the <sup>13</sup>C pocket (see Bisterzo et al. 2014, their Fig. 4). Note that *s*-only isotopes with  $A < 90$  (<sup>70</sup>Ge, <sup>76</sup>Se, <sup>80,82</sup>Kr, <sup>86,87</sup>Sr) receive an additional contribution by the weak *s*-process in massive stars (see e.g., Pignatari et al. 2010).

contribution to light isotopes with  $A = 96 - 130$  is favored. As suggested by Maiorca et al. (2012) and Cristallo et al. (2015), it is crucial to verify that the delayed contribution of metal-rich AGB stars to the solar epoch is properly considered in the framework of our GCE model. Otherwise, the solar LEPP-s may derive from a relevant underestimation of the metal-rich AGB component.

The theoretical minimum AGB initial mass that can contribute to the solar system is rather uncertain and model dependent. In our GCE computations,  $M \leq 1.3 M_{\odot}$  models with  $[\text{Fe}/\text{H}] \gtrsim -0.4$  do not contribute to the chemical evolution of the Galaxy because the conditions for the activation of the TDU episodes are never reached in our models (see e.g., Bisterzo et al. 2014, and references therein).

We have analyzed here a test case, in which we have accounted for the longest life of the AGB stars that may contribute to the solar distribution (e.g., our  $1.3 M_{\odot}$  models with disc metallicity have lifetime of  $\sim 4$  Gyr). In Fig. 2 (bottom panel), we compare the  $s$  distribution obtained at the formation time of the solar system ( $t_{\odot} = 9.2$  Gyr) and that computed at  $t_{Gal} = 13.1$  Gyr, in which the overall metal-rich AGB component that may contribute to the solar  $s$  distribution is included. The two distributions show marginal variations ( $\lesssim 3\%$ ) for  $A > 90$ . Indeed, our GCE model adopts a very efficient star formation rate in the halo, which produces a fast metallicity increase at the early evolutionary epochs ( $[\text{Fe}/\text{H}] = -2$  at 0.1 Gyr). An extended thin disc phase ( $\sim 8$  Gyr) assures that the contribution of metal-rich stars is not overlooked. Moreover, the small star formation rate after 9.2 Gyr results in a slow metallicity increase (by +0.11 dex from solar to 13.1 Gyr). For this reason, the solar distribution (normalized to  $^{150}\text{Sm}$ ) shows small variations at the two selected epochs. This indicates that the solar distribution properly accounts for the contribution of AGB yields with  $[\text{Fe}/\text{H}] \lesssim -0.2$ .

Non-negligible variations are found for  $^{86,87}\text{Sr}$  and  $^{89}\text{Y}$ : at  $t_{Gal} \sim 13$  Gyr,  $\Delta(^{86,87}\text{Sr}) \simeq +8\%$  and  $\Delta(^{89}\text{Y}) \simeq +4\%$ . The  $s$ -only isotopes with  $A < 90$  are mainly produced by AGB stars

with  $[\text{Fe}/\text{H}] \sim -0.15$ , which corresponds to  $t_{\text{Gal}} \sim 6.3$  Gyr, only about 2.9 Gyr before the solar system formation (see Fig. 2, top panel). This is comparable to the lifetime of AGB stars with  $M = 1.4 - 1.5 M_{\odot}$  with  $[\text{Fe}/\text{H}] \sim -0.15$  ( $t_{\star} \sim 3.0$  to 2.4 Gyr, respectively).

In Table 2, we list the  $s$  contributions to elements from Sr to Cd at  $t_{\odot} = 9.2$  Gyr and  $t_{\text{Gal}} \sim 13$  Gyr: although non-negligible variations are found for Sr (+5%) and Y (+4%), these differences are compatible with the solar uncertainties. As discussed in the previous Section, the LEPP-s is still required.

#### 4. GCE $s$ - and $r$ -process contributions versus $[\text{Fe}/\text{H}]$

In this section we present our results for the chemical evolution of selected neutron-capture elements as a function of metallicity. We analyze the chemical evolution of Y, Zr, Ba, La and Pb (representative of the three  $s$ -process peaks), and Eu (typical of the  $r$ -process elements). GCE predictions are compared with updated high-resolution spectroscopic observations.

The Galactic enrichment of the three  $s$ -process peaks is followed by accounting for the  $s$ -process AGB yields discussed in Sections 2 and 3. An additional contribution to the first  $s$  peak is ascribed to the ‘classical’ weak  $s$  component from (non-rotating) massive stars (Raiteri, Gallino & Busso 1992; Pignatari et al. 2010). Given the secondary-like nature of the  $^{22}\text{Ne}(\alpha, n)^{25}\text{Mg}$  neutron source in standard non-rotating massive stars (with yields scaling quite linearly with the initial metallicity), the weak  $s$  process is mainly relevant at solar metallicity, accounting for up to  $\sim 10\%$  of solar Sr-Y-Zr (Travaglio et al. 2004). We will discuss the supplementary impact of fast-rotating low-metallicity massive stars on GCE predictions in Section 4.1.

Concerning the treatment of Eu and  $r$ -process elements, we have adopted the same prescription discussed by Travaglio et al. (1999). Actually, the origin of the  $r$  process is still

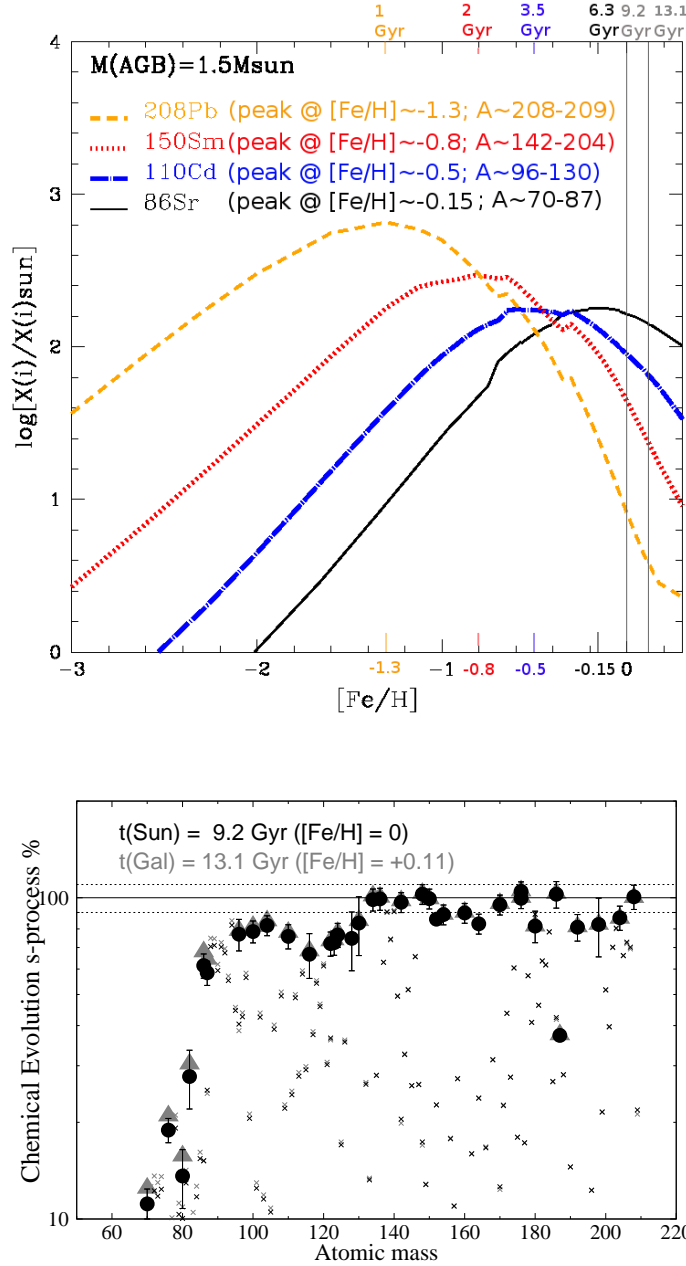


Fig. 2.— Top panel: AGB yields (obtained with a weighted average of standard  $^{13}\text{C}$ -pockets) of a  $1.5 M_{\odot}$  model at different metallicities. Four selected  $s$ -only isotopes are shown:  $^{150}\text{Sm}$  is representative of heavy  $s$ -only isotopes with  $A = 142 - 204$  (peaked at  $[\text{Fe}/\text{H}] \sim -0.8$ , which in our GCE model corresponds to a Galactic time of  $t_{\text{Gal}} \sim 2$  Gyr);  $^{110}\text{Cd}$  illustrates the behavior of light  $s$ -only isotopes with  $A = 96 - 130$  ( $[\text{Fe}/\text{H}] \sim -0.5$ ;  $t_{\text{Gal}} \sim 3.5$  Gyr); last are the  $s$ -only isotopes with  $A = 70 - 87$ , represented by  $^{86}\text{Sr}$  ( $[\text{Fe}/\text{H}] \sim -0.15$ ;  $t_{\text{Gal}} \sim 6.3$  Gyr).  $^{208}\text{Pb}$  is efficiently produced by low-metallicity AGB stars ( $[\text{Fe}/\text{H}] \sim -1.3$ ;  $t_{\text{Gal}} \sim 1$  Gyr). Bottom panel: the  $s$ -process distribution obtained at the epoch of the solar system formation ( $t_{\odot} = 9.2$  Gyr at  $[\text{Fe}/\text{H}] = 0$ ; black symbols) compared with the  $s$ -process distribution obtained at a Galactic time of  $t_{\text{Gal}} = 13.1$  Gyr (at  $[\text{Fe}/\text{H}] = +0.11$ ; gray symbols).

unclear and largely uncertain. Spectroscopic observations have evidenced the existence of multiple  $r$ -process components operating in the early Galaxy (see, e.g., Siqueira Mello et al. 2015; Roederer et al. 2014; Hansen et al. 2014a, 2012; Peterson 2013; Montes et al. 2007, and references therein). At least two  $r$ -processes have been proposed: the main  $r$  process ( $A > 130$ ), which is currently ascribed to mergers of compact objects and/or magneto-rotationally driven supernovae, and the weak  $r$  process (or  $\nu$ p-process, rp-process;  $A \sim 80$  to 120), which has been proposed as an alternative nucleosynthesis source of lighter heavy elements in neutrino-driven supernova outflows. Noteworthy progresses have been reached in modeling these extremely energetic and complex events, but the unclear physical conditions of the astrophysical sites and the inaccessibility of nuclear physics inputs lead to very uncertain  $r$ -process predictions (see e.g., Pereira & Montes 2016; Eichler et al. 2015; Goriely et al. 2015; Nishimura et al. 2015; Kratz, Farouqi & Moller 2014; Winteler et al. 2012; Arcones & Thielemann 2013; Qian & Wasserburg 2008, and references therein). The lack of a comprehensive  $r$ -process view forced us to systematically include an  $r$ -process contribution in GCE computations. For elements heavier than Ba, the solar  $r$ -process contribution is derived by subtracting the  $s$  fractions from the solar abundances (the so-called  $r$ -process residuals method; Käppeler et al. 1982, 2011). Following the observed decreasing trend of heavy neutron-capture elements in the early Galaxy, we ascribe the  $r$  contribution to a primary process occurring in SNII with a limited range of progenitor masses,  $M \sim 8\text{--}10 M_{\odot}$  (Travaglio et al. 1999). In light of the present uncertainties, we do not exclude different hypotheses (e.g., Jet-SNe, neutron star mergers). Chemo-dynamical evolution models are needed to adequately explore the chemical origin of an inhomogeneous Galactic halo (see e.g., discussion by Shen et al. 2015; van de Voort et al. 2015; Kobayashi & Nakasato 2011). Nevertheless, by adopting different ranges of stellar mass progenitors for the  $r$  process, the GCE predictions show marginal variations for disk metallicities, and for the solar  $s$  distribution.

Even more puzzling is the origin of light neutron-capture elements in the early Galaxy, for which simple  $r$ -process residuals provide inadequate descriptions (Travaglio et al. 2004). Accordingly, a different treatment is required

for Sr, Y and Zr. We derive an  $r$  fraction of  $\sim 10\%$  from observations of very metal-poor  $r$ -rich stars (Mashonkina & Christlieb 2014; Roederer et al. 2014), under the hypothesis that these peculiar objects show the signature of a pure main  $r$ -process. An additional LEPP contribution was evoked by Travaglio et al. (2004) to explain the missing abundances of solar Sr, Y, and Zr. The flat  $[\text{Sr}, \text{Y}, \text{Zr}/\text{Fe}]$  trend observed at low metallicities suggests that LEPP is a primary process, likely occurring in SNII with an extended range of mass progenitors compared to the main  $r$  process. As discussed by Travaglio et al. (2004), we confirm that the solar LEPP-s described in Section 2 and the metal-poor LEPP may originated in different stellar environments.

Figures 3 and 4 illustrate the Galactic evolution of  $[\text{Ba}/\text{Fe}]$ ,  $[\text{La}/\text{Fe}]$ ,  $[\text{Y}/\text{Fe}]$ ,  $[\text{Zr}/\text{Fe}]$ ,  $[\text{Eu}/\text{Fe}]$ ,  $[\text{Pb}/\text{Fe}]$  and their ratios  $[\text{Ba}/\text{Eu}]$ ,  $[\text{La}/\text{Eu}]$ ,  $[\text{Eu}/\text{Y}]$ ,  $[\text{Eu}/\text{Zr}]$ ,  $[\text{Ba}/\text{Y}]$ ,  $[\text{Pb}/\text{Eu}]$  versus  $[\text{Fe}/\text{H}]$ .

Spectroscopic observations are taken from Aoki & Honda (2008; *dark-green filled-diamonds*), Nissen & Schuster (2011; *big-empty circles*), Andrievsky et al. (2011; *red squares*), Aoki et al. (2013; *light-gray squares*), Hansen et al. (2012; *brown and sienna empty squares* for dwarfs and giants, respectively), Hansen et al. (2014b; *black asterisks*), Roederer et al. (2010, 2012, 2014, 2014a; *blue stars, dark-green and green squares, gray filled-circles*), Ishigaki et al. (2013; *green, orange, and violet right-rotated triangles* for thick-disc, inner-halo and outer-halo stars, respectively), Mishenina et al. (2013; *light-blue and sienna squares* for thin and thick disc stars, respectively), Cohen et al. (2013; *magenta asterisks*), Yong et al. (2013; *blue hexagons*), Bensby et al. (2014) and Battistini & Bensby (2016; *red, blue, magenta, purple triangles* for thin disc stars, unclassified stars,

thick-disc and halo stars, respectively), Mashonkina et al. (2014; *black triangles*), Siqueira Mello et al. (2014; *black down-rotated triangles*). Stars with  $[\text{Ba}/\text{Fe}] \geq +0.6$  and  $[\text{Ba}/\text{Eu}] > 0$  are excluded (e.g., possible binaries as Ba stars, C-stars, CEMP-s stars). The well studied sample of  $r$ -rich stars at  $[\text{Fe}/\text{H}] < -2.2$  (r-I and r-II stars, with  $[\text{Eu}/\text{Fe}] \geq 1$  and  $[\text{Ba}/\text{Eu}]_{\text{r}} \sim -0.8$ ; Mashonkina & Christlieb 2014; Roederer et al. 2014; Siqueira Mello et al. 2014) are peculiar objects likely born from a cloud polluted by a pure  $r$ -process production event. They do not represent the average chemical evolution of our Galaxy.

GCE predictions account for the  $s$ -process, the  $r$ -process, and the LEPP contributions, in the halo, thick disk, and thin disk (*dotted*, *dashed* and *full lines*, respectively). AGB yields with a standard  $^{13}\text{C}$ -pocket choice (first group of data in Table 1) are included. The shaded area at  $[\text{Fe}/\text{H}] \leq -2.5$  indicates that homogeneous GCE models can not properly represent the  $[\text{El}/\text{Fe}]$  scatter observed in the early Galaxy for neutron-capture elements. It is noteworthy that low  $[\text{Sr}, \text{Ba}, \text{Eu}/\text{Fe}]$  abundances in metal-poor field stars may be affected by higher uncertainties owing to observational detection thresholds (Roederer et al. 2013, 2014a).

In Figure 5, we illustrate the impact of AGB yields computed with different  $^{13}\text{C}$ -pocket tests selected from Section 2 on GCE predictions of  $s$ -process elements. We consider  $[\text{Ba}/\text{Fe}]$ ,  $[\text{Y}/\text{Fe}]$  and  $[\text{Pb}/\text{Fe}]$  versus  $[\text{Fe}/\text{H}]$  as representative of the three  $s$  peaks. Similar results are obtained for  $[\text{La}/\text{Fe}]$  and  $[\text{Zr}/\text{Fe}]$ .

As discussed in Section 2,  $[\text{El}/\text{Fe}]$  and their ratios are plausibly reproduced at  $[\text{Fe}/\text{H}] = 0$ . Variations up to  $\Delta[\text{El}/\text{Fe}] \sim \pm 0.2$  dex are shown by GCE predictions of the three  $s$  peaks in the metallicity range of  $-1.6 < [\text{Fe}/\text{H}] < 0.1$ . At  $[\text{Fe}/\text{H}] < -1.6$ , the  $s$  contribution is negligible, and marginal variations are expected. Eu, which receives a dominant  $r$ -process contribution (94%), is unaffected by different tests.

The growing number of spectroscopic data currently suggests a possible underestimation



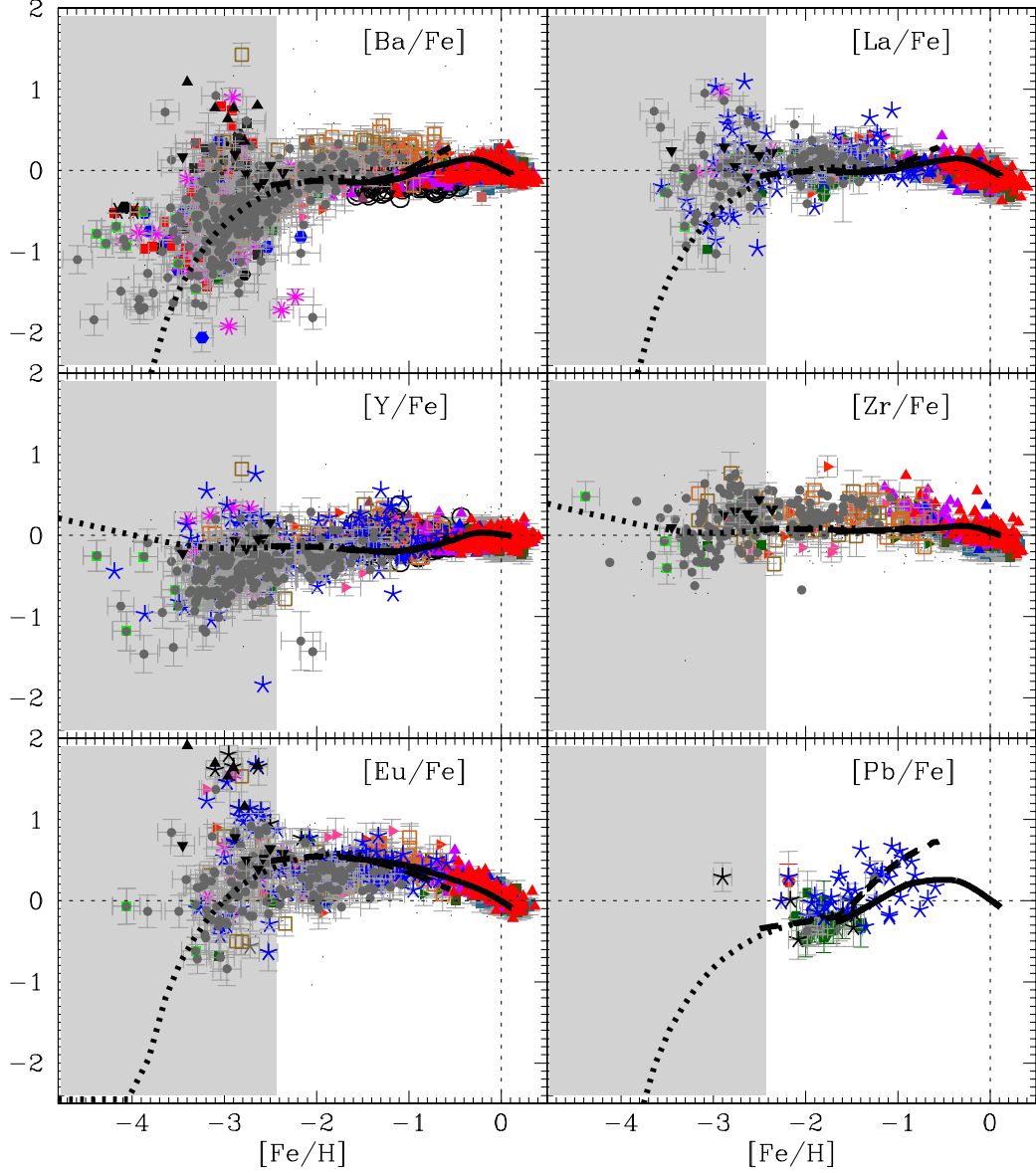


Fig. 3.— GCE s- and r-process contributions of  $[\text{Ba}/\text{Fe}]$ ,  $[\text{La}/\text{Fe}]$ ,  $[\text{Y}/\text{Fe}]$ ,  $[\text{Zr}/\text{Fe}]$ ,  $[\text{Eu}/\text{Fe}]$ , and  $[\text{Pb}/\text{Fe}]$  versus  $[\text{Fe}/\text{H}]$ . Different lines correspond to GCE results for halo (*dotted lines*), thick and thin discs (*dashed* and *full lines*, respectively) obtained with a standard choice of the  $^{13}\text{C}$ -pocket (Table 1). References and symbols for spectroscopic observations are given in the text.

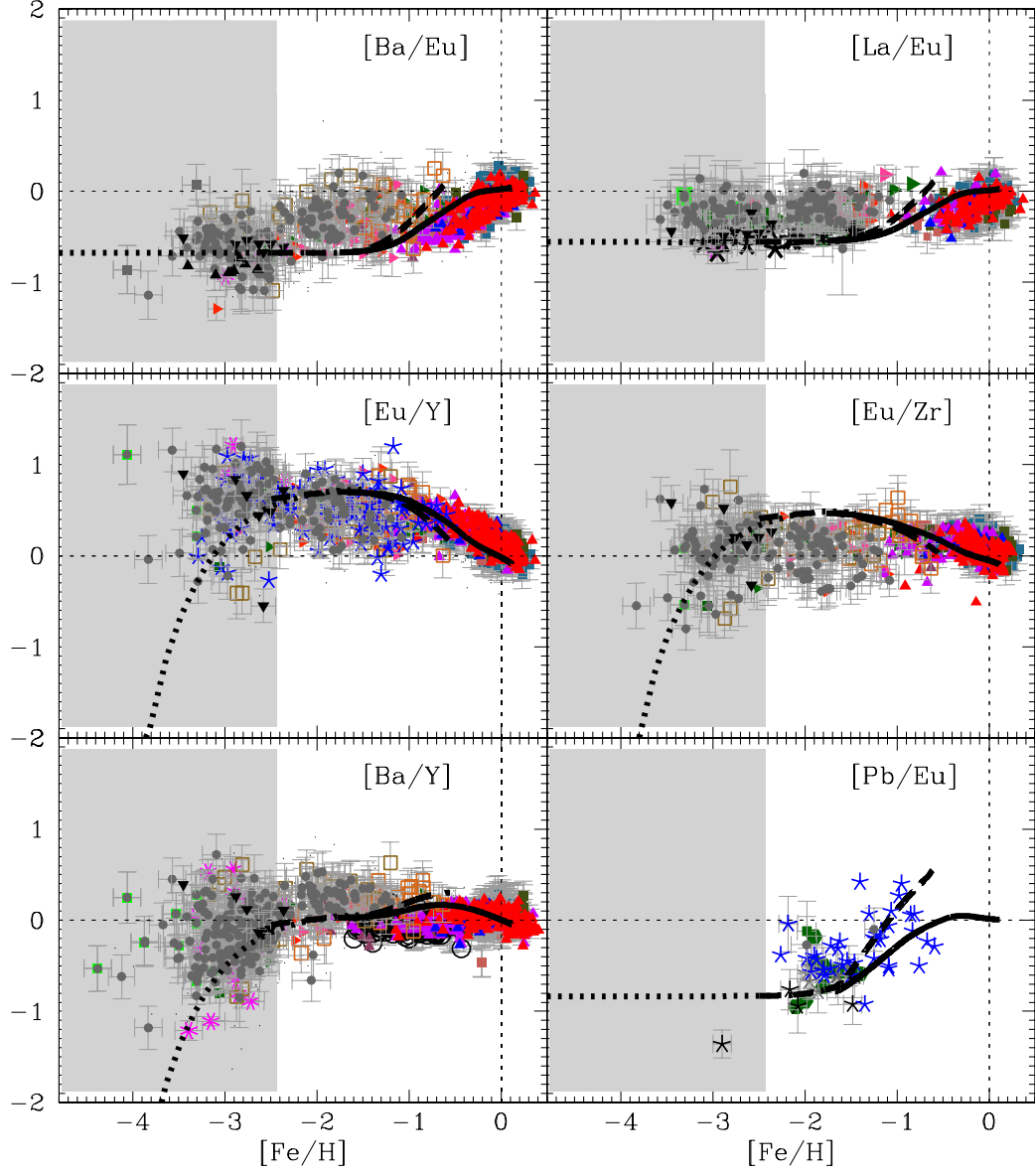


Fig. 4.— The same as Fig. 3, but for  $[\text{Ba}/\text{Eu}]$ ,  $[\text{La}/\text{Eu}]$ ,  $[\text{Eu}/\text{Y}]$ ,  $[\text{Eu}/\text{Zr}]$ ,  $[\text{Ba}/\text{Y}]$  and  $[\text{Pb}/\text{Eu}]$  versus  $[\text{Fe}/\text{H}]$ .

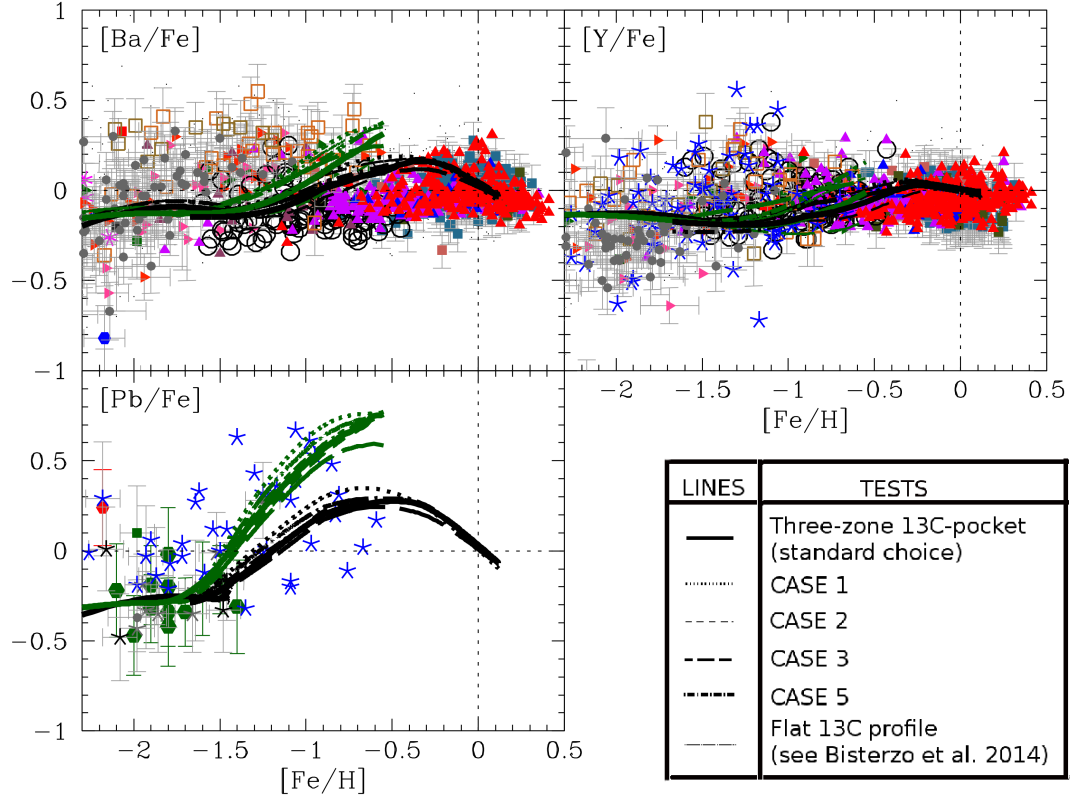


Fig. 5.— GCE contributions of  $[\text{Ba}/\text{Fe}]$ ,  $[\text{Y}/\text{Fe}]$  and  $[\text{Pb}/\text{Fe}]$  versus  $[\text{Fe}/\text{H}]$ . Different lines correspond to GCE results for thick (*green lines*) and thin disc (*black lines*) obtained with different  $^{13}\text{C}$ -pocket tests in Table 1. We also display the result of a flat  $^{13}\text{C}$ -pocket profile obtained by excluding the two external  $^{13}\text{C}$ -rich zones of the pocket (see Bisterzo et al. 2014). Spectroscopic observations are the same shown in Fig. 3.

of the observed  $[\text{Ba}/\text{Fe}]$  for  $[\text{Fe}/\text{H}] \sim -2$ , independently of the  $^{13}\text{C}$  profile adopted in the pocket. For instance, the observed  $[\text{Ba}/\text{Eu}]$  ratio smoothly increases starting from  $[\text{Fe}/\text{H}] \sim -2.5$  (Roederer et al. 2014a; Ishigaki et al. 2013; Hansen et al. 2012), about 1 dex earlier than predicted by our model ( $[\text{Fe}/\text{H}] \sim -1.6$ ). Despite a smaller dispersion is observed for  $[\text{La}/\text{Fe}]$ , similar indications are given by  $[\text{La}/\text{Eu}]$ , which on average show an even flatter and higher trend for  $[\text{Fe}/\text{H}] < -2$ . This trend appears a characteristic of the second  $s$  peak rather than other  $s$  elements (see, e.g.,  $[\text{Y}, \text{Zr}/\text{Fe}]$  and  $[\text{Ba}/\text{Y}]$  versus  $[\text{Fe}/\text{H}]$ ). Otherwise, Galactic thin and thick disk dwarfs by Mishenina et al. (2013; little filled squares in the metallicity range of  $-1 \leq [\text{Fe}/\text{H}] \leq +0.3$ ) show a delayed and steeper  $[\text{Ba}, \text{La}/\text{Eu}]$  increase, in agreement with our GCE  $s$  process enrichment.

Current AGB yields seem not give adequate hints to account for this behavior. Within a GCE framework, several studies agree that the rise of the AGB  $s$  process occurs beyond  $[\text{Fe}/\text{H}] \sim -1.6$  (Matteucci et al. 2009; Kobayashi & Nomoto 2009), given the fast iron enrichment occurring in the early Galaxy. However, an anticipated rise for the  $s$ -process was questioned by previous spectroscopic studies (Simmerer et al. 2004; Hansen et al. 2012).

Recent observational and theoretical studies have evidenced that an additional intermediate neutron-capture process (the  $i$  process) may play an important role in the evolution of the Galaxy (see, e.g., peculiar chemical signatures discussed by Roederer et al. 2016; Mishenina et al. 2015; Dardelet et al. 2015; Lugaro et al. 2015; Jadhav et al. 2013; Liu et al. 2014). Despite its existence was hypothesized 30 years ago by Cowan & Rose (1977), observational hints have only recently been revealed. The  $i$  process occurs when protons are ingested in He-burning convective stellar regions to form  $^{13}\text{C}$ , which is the main source of neutrons via the  $(\alpha, n)$  reaction, driving neutron densities of  $\sim 10^{15}$  neutrons  $\text{cm}^{-3}$ . The physical conditions leading to the  $i$  process may be found in different stellar environments, as super-AGB and post-AGB stars, He-core and He-shell flashes in low-metallicity low-mass stars, and massive stars (Cristallo et al. 2009; Herwig et al. 2011;

Stancliffe et al. 2011; Jones et al. 2016; Woodward, Herwig & Lin 2015). Improved stellar models with the guidance from hydrodynamics simulations will help to establish the impact of the  $i$  process in the Milky Way.

#### 4.1. The impact of rotating-massive stars on GCE predictions of $s$ -process elements

The important contribution of fast-rotating massive stars in the early Galaxy has been evidenced by several studies (see e.g., the review by Maeder & Meynet 2012). First investigations highlighted that rotational induced-mixing boost the production of primary  $^{14}\text{N}$  in the H-burning shell, subsequently converted to  $^{22}\text{Ne}$  via  $2\alpha$  captures in the He-burning core (Meynet, Ekström & Maeder 2006; Hirschi 2007). The large amount of  $^{22}\text{Ne}$  primarily produced at low metallicities leads to an efficient nucleosynthesis of light  $s$  elements, and may extend up to the barium peak (Pignatari et al. 2008). The recent studies by Frischknecht, Hirschi, & Thielemann (2012) and Frischknecht et al. (2016) show a large sensitivity of the first two  $s$  peaks to both metallicity and rotation, with a  $[\text{Sr}/\text{Ba}]$  predicted ratio that covers more 2 dex in most metal-free models. Rotating low-metallicity massive stars are a promising site to explain the  $[\text{Sr}/\text{Ba}]$  dispersion observed in the halo. Chiappini et al. (2011) first advanced the hypothesis that metal-poor fast-rotating massive stars may offer a plausible explanation for the large  $[\text{Ba}/\text{Y}]$  dispersion observed in the early Universe. Later on, the inhomogeneous chemical evolution model by Cescutti et al. (2013) provided a quantitative estimation in support of this hypothesis.

The aim of this Section is to test the effect of weak  $s$  process yields from fast-rotating massive stars on GCE predictions of  $s$ -process elements. Specifically, new yields by Frischknecht et al. (2016) are analyzed in the framework of our GCE model in order to explore the impact on the solar and metal-poor LEPP mechanisms.

Frischknecht et al. (2016) provide a grid of four stellar masses ( $M = 15, 20, 25$  and  $40 M_{\odot}$ ) and three metallicities ( $Z = Z_{\odot}, 10^{-3}, 10^{-5}$ ), computed with a full s-process network. We have linearly interpolated the weak  $s$  yields between the mass range of  $15 < M/M_{\odot} \leq 40$  and the metallicity range. The authors compare non-rotating and standard-rotating models ( $v_{ini}/v_{crit} = 0.4$ , where the critical velocity  $v_{crit}$  assumed by the authors corresponds to an average equatorial velocity of  $\sim 200 \text{ km s}^{-1}$  on the main sequence at  $Z_{\odot}$ , and increases to  $\sim 400 \text{ km s}^{-1}$  at low metallicity, see Frischknecht, Hirschi, & Thielemann 2012). They also provide additional yields on the  $25 M_{\odot}$  model down to  $Z = 10^{-7}$ , with fast-rotation rates ( $v_{ini}/v_{crit} = 0.5$  and  $0.6$ , with  $v_{crit}$  up to  $\sim 590 \text{ km s}^{-1}$ ). For fast-rotating low-metallicity models of  $25 M_{\odot}$ , the authors discussed a further test in which the  $^{17}\text{O}(\alpha, \gamma)$  rate is divided by a factor of ten, in better agreement (within the uncertainties) with the recent measurement by Best et al. (2013).

Although only pre-explosive SN yields are given by Frischknecht et al. (2016), they are suited for GCE studies because strong variations on the total yields of s-process nuclei are not expected after SN explosion (see e.g., Tur, Heger & Austin 2014).

We have considered three tests:

- a first test with non-rotating weak  $s$ -process yields (label  $NR$ ; corresponding to models ‘s0’ in Table 1 by Frischknecht et al. 2016), which provides a more exhaustive analysis of the ‘classical’ weak- $s$  process contribution included in the GCE predictions presented in Section 4;
- a second test with standard-rotating weak  $s$ -process yields (label  $SR$ ; corresponding to models ‘s4’ in Table 1 by Frischknecht et al. 2016, with  $v_{ini}/v_{crit} = 0.4$ );
- the same as the second test, but with fast-rotating yields ( $v_{ini}/v_{crit} = 0.6$ ;  $FR$ ) coupled with the  $^{17}\text{O}(\alpha, \gamma)$  rate divided by a factor of ten for the  $25 M_{\odot}$  model at  $Z = 10^{-5}$  and  $10^{-7}$  (corresponding to models ‘s6b’ in Table 1 by Frischknecht et al. 2016). We applied the same scaling factors to  $40 M_{\odot}$  models.

In Fig. 6, the impact of new weak  $s$  yields is shown for the solar abundance distribution of  $s$  isotopes. Non-rotating weak  $s$  yields mainly increase the solar abundances of isotopes with  $A \lesssim 80$ , with a small contribution to Sr, Y and Zr. This is in agreement with previous ‘classical’ analyses, which have been obtained starting from the solar weak  $s$  contribution and following a secondary-like behavior by decreasing the metallicity. Fast-rotating models produce an evident increase of isotopes lighter than  $A \lesssim 90$ , with an additional contribution of  $\sim 30\%$  to  $^{86,87}\text{Sr}$ , and  $\sim 10\%$  to  $^{89}\text{Y}$ ,  $\sim 5\%$  to  $^{90,91,92}\text{Zr}$  among non  $s$ -only isotopes. This corresponds to a weak  $s$  contribution from fast-rotating massive stars of about 17%, 10% and 5% to solar Sr, Y, Zr, respectively. In the atomic mass region between  $90 < A < 140$ ,  $s$ -only isotopes are marginally affected, with variations within the solar uncertainties. This suggests that fast-rotating massive stars may only partially account for the solar LEPP, being inefficient for  $A > 90$ .

By considering the influence of the fast-rotating weak- $s$  process over the whole Galactic enrichment, we display in Fig. 7 the impact on  $[\text{Ba}/\text{Fe}]$ ,  $[\text{Y}/\text{Fe}]$ ,  $[\text{Ba}/\text{Y}]$  and  $[\text{Eu}/\text{Y}]$  versus  $[\text{Fe}/\text{H}]$ , selected as most representative. Black lines account for both the ‘classical’ weak- $s$  process and for the estimated LEPP. Other lines are computed by setting the LEPP contribution to zero, and by including the three tests listed above for the weak- $s$  process. We adopt our standard treatment described in Section 4 for the  $r$  contribution. The  $r$  process dominates the  $[\text{Ba}/\text{Fe}]$  predictions for  $-3 \leq [\text{Fe}/\text{H}] \lesssim -1.5$ . The impact of fast-rotating models only affects very metal-poor GCE predictions (see *red line* at  $[\text{Fe}/\text{H}] < -3$ ). As expected, Eu (which is not shown in Figure) does not present variations. For  $[\text{Y}/\text{Fe}]$ , different initial rotation rates (represented by *green*, *blue*, and *red* lines in Fig. 7) seem to cover a more extended range of stellar observations at  $[\text{Fe}/\text{H}] < -3$ . This also partly explains the observed  $[\text{Eu}/\text{Y}]$  and  $[\text{Ba}/\text{Y}]$  dispersions. It is noteworthy that fast-rotating massive stars offer a promising nucleosynthesis site for the metal-poor LEPP. For instance, GCE predictions that account for fast-rotating weak- $s$  process yields (*red line*) move towards

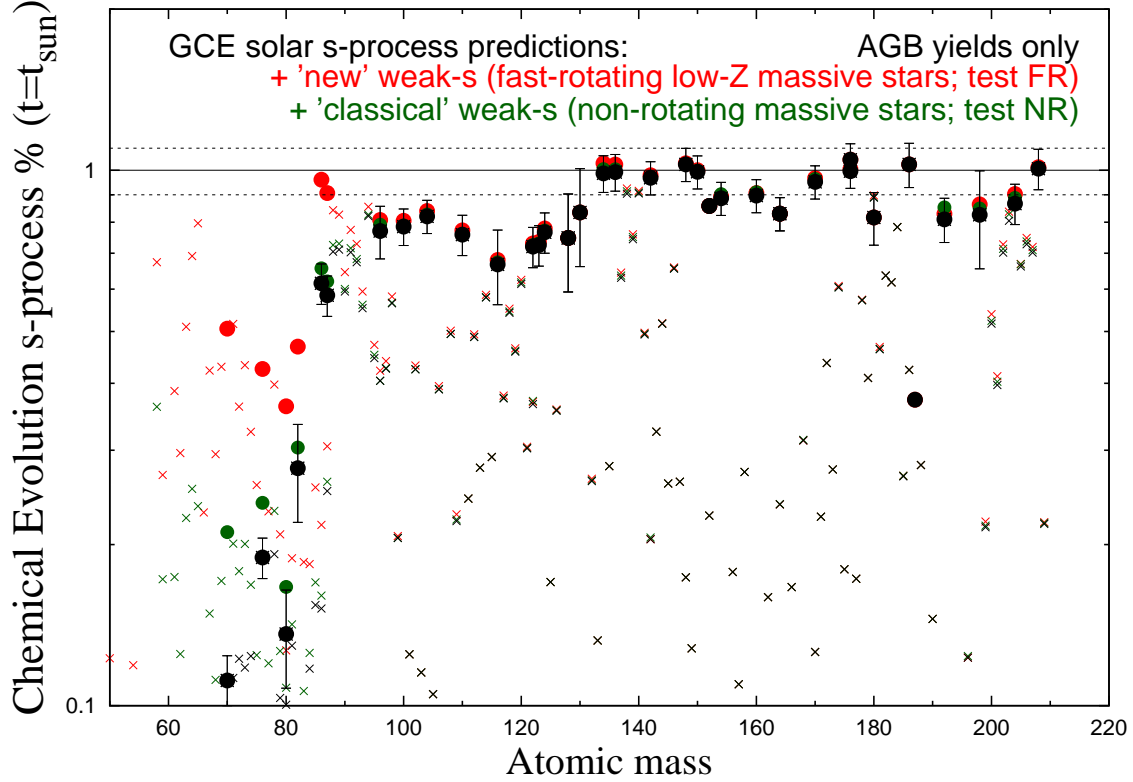


Fig. 6.— Effect of rotating-massive stars on GCE predictions of  $s$ -process elements. Black symbols stand for the standard GCE results obtained in Fig. 1. GCE predictions computed with non-rotating weak  $s$  yields are represented with *green symbols* (test  $NR$ ). GCE results that include fast-rotating models and the  $^{17}\text{O}(\alpha, \gamma)$  rate divided by a factor of ten are displayed with *red symbols* (test  $FR$ ). See text for more details.



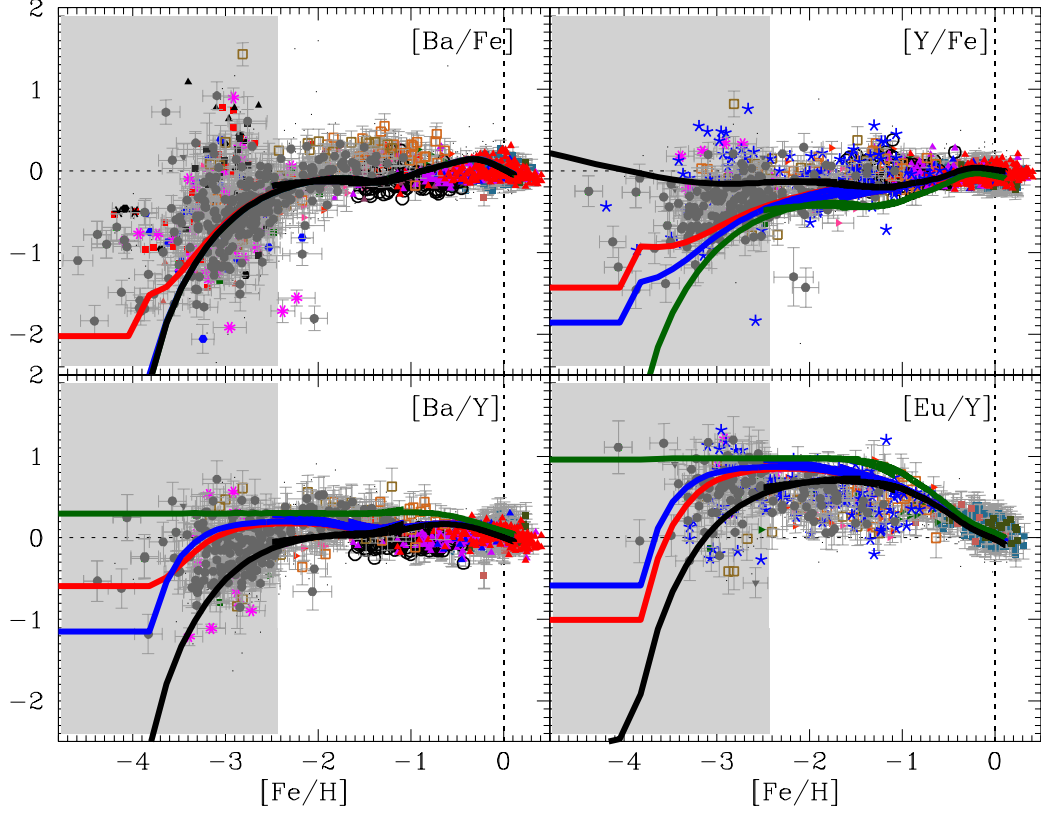


Fig. 7.— Observations  $[\text{Ba}/\text{Fe}]$ ,  $[\text{Y}/\text{Fe}]$  and the ratios  $[\text{Ba}/\text{Y}]$ ,  $[\text{Eu}/\text{Y}]$  versus  $[\text{Fe}/\text{H}]$  are compared with GCE predictions computed with different weak  $s$  process contributions. Black lines represent the same GCE predictions shown in Figs 3 and 4, in which the ‘classical’ weak- $s$  process is included. Other lines show GCE results obtained by testing the weak- $s$  process yields recently provided by Frischknecht et al. (2016) for massive stars with different initial rotation rates: non-rotating (*green lines*; test *NR*) and standard-rotating models (*blue lines*; test *SR*), and fast-rotating models coupled with the  $^{17}\text{O}(\alpha, \gamma)^{21}\text{Ne}$  rate divided by a factor of ten (*red lines*; test *FR*).

the original model with the estimated LEPP (*black* line). Although our homogeneous GCE model can not provide a realistic representation of the observed s-element dispersion, the averaged GCE predictions shown in Fig. 7 are in agreement with previous results presented by Cescutti et al. (2013), who indicated that low-metallicity fast-rotating massive stars may reproduce the [Sr/Ba] inhomogeneities observed in extremely metal-poor stars.

Note that large uncertainties affect massive-star models, as discussed by Frischknecht et al. (2016): on the nuclear point of view, owing to the uncertain  $^{17}\text{O}+\alpha$  and  $^{22}\text{Ne}+\alpha$  rates, and on the modeling point of view, mainly because of the treatment of the physics associated to magnetic fields and rotation-induced mixing. In the framework of GCE models, a more detailed grid of stellar yields may help to better assess an upper limit for the fast-rotating weak-s process contribution.

As evidenced by different GCE approaches, the chemical enrichment of the stellar halo is likely the result of a merger of different (primary) processes, including fast-rotating weak-s process and  $r$  processes (e.g., Ishimaru & Wanajo 1999; Argast et al. 2004; Cescutti 2008; Matteucci et al. 2014; see also Section 4).

## 5. Conclusions

We have implemented the study on GCE predictions of  $s$ -process elements presented by Bisterzo et al. (2014) by including recent pivotal suggestions provided in literature.

The main result is that the predicted chemical compositions in the interstellar medium at any epoch are grossly independent of the particular  $^{13}\text{C}$  profile adopted inside the pocket, once a different weighted average of  $^{13}\text{C}$ -pocket strengths is considered to reproduce solar  $^{150}\text{Sm}$  (within 5% accuracy).

The impact of AGB uncertainties on GCE computations may be partially reduced by assuming a range of  $^{13}\text{C}$ -pocket strengths, as indicated by observational constraints.

Actually, this approach allows us to obtain more accurate information about the complementary contribution from other nucleosynthesis processes that may compete over the Galactic history. In the framework of these  $^{13}\text{C}$ -pocket prescriptions, we confirm that the additional LEPP-s mechanism invoked by Travaglio et al. (2004) is required to represent the observed solar distribution within the estimated solar uncertainties. In this view, only 3D or hydrodynamical AGB modeling may shed light on the  $^{13}\text{C}$ -pocket scenario.

Updated GCE calculations accounting for recent fast-rotating metal-poor weak  $s$ -process yields by Frischknecht et al. (2016) may partially solve the missing contribution to the solar Sr-Y-Zr abundances. The [Sr/Ba] dispersion observed in the early Galaxy may be reconciled with the contribution of metal-poor massive stars with different rotational velocity, in agreement with previous results by Chiappini et al. (2011) and Cescutti et al. (2013). A more detailed grid of stellar yields would help to assess the total  $s$  contribution. From the present analysis, a combination of different  $r$  and  $s$  process components is the most promising scenario to explain the solar and the metal-poor LEPP.

In this view, additional processes have to be invoked to explain the observed trends. The intermediate neutron-capture process ( $i$  process) may play a decisive role in the nucleosynthesis of the Galaxy (see Roederer et al. 2016; Mishenina et al. 2015, and references therein).

This issue deserves a more comprehensive analysis in order to establish whether the present discrepancies between GCE predictions and the analyzed spectroscopic sample are confirmed by other elements. Future investigations with a more extended and homogeneous data-set of neutron-capture elements (e.g., Cu, Ga, Ge, among weak  $s$  process elements; Mo, Ru, Ag, Pd, for weak  $r$  process elements; Ce, which is expected to behave as Ba) are planned to distinguish between different nucleosynthesis processes.

The improved quality and statistics of the ongoing surveys (e.g., GAIA-ESO, SEGUE,

RAVE, APOGEE, HERMES-GALAH) will also assure a more solid picture of the Galactic sub-structures. First studies by Edvardsson et al. (1993), Reddy et al. (2003) and Bensby et al. (2003) evidenced that stars belonging to the thin and thick discs have different ages, kinematics, locations on the Galactic plane, and chemical properties. Although a complex image of the Galactic structure emerges from the most recent investigations (e.g., perturbation, accretion, merging or heating processes, radial migrations, gas flows; see the review by Rix & Bovy 2013), the main features observed in the solar neighborhood are confirmed by several surveys. For instance, it has been well established in literature that various  $\alpha$ -elements show clear separate behaviors in the thick and the thin disc.

In this view, a detailed analysis of our GCE prescriptions is required in order to provide an improved representation of the chemical abundances observed in thick/thin disc stars (see, e.g., [O/Fe] vs [Fe/H] in Fig. 1 by Bisterzo et al. 2014).

A preliminary study of the main GCE ingredients (e.g., star formation rate, initial mass function, delay-time distribution function for SNIa, and the present uncertainties affecting SNIa stellar yields) highlights that the theoretical interpretation of the thick/thin disc observed trends is largely affected by the poorly known SNIa scenario (see, e.g., Maoz, Mannucci & Nelemans 2014; Ruiz-Lapuente 2014; Travaglio et al. 2015; Marquardt et al. 2015; Hillebrandt et al. 2013; Ruiter, Belczynski, & Fryer 2009, and references therein). Specifically, our GCE thick/thin disc predictions may be improved by assuming a factor of 2 uncertainty in the SNIa stellar yields adopted so far (Travaglio, Hillebrandt & Reinecke 2005), coupled with an updated treatment of the delayed-time distribution (DTD) function (as suggested by Kobayashi et al. 1998; Greggio 2005; Matteucci et al. 2009; Kobayashi, Nomoto, & Hachisu 2015), in which we assume a dominant SNIa contribution starting from  $[\text{Fe}/\text{H}] > -1$ .

Additionally, distinct enrichment histories of the thick/thin disc components may be obtained by adopting a different star formation rate, with a delayed thin disc phase (as

hypothesized by the two-infall model by Chiappini et al. 1997). To this purpose, we will provide a comprehensive investigation of several GCE ingredients against a large number of elements in a forthcoming paper. The underway study of SNIa yields for an extended metallicity grid will further constraint the disc chemical enrichment. New SNIa inputs, combined with high-resolution studies of several chemical elements and the reliable age determination expected from astroseismology (CoRoT and Kepler, Anders et al. 2016; Stello et al. 2015), will provide a real breakthrough in the understanding of the Galactic history.

It is noteworthy that we will extend the analysis to young open clusters, which are mandatory to understand the chemical evolution of neutron-capture elements in the Galactic disc (Maiorca et al. 2012; Mishenina et al. 2015).

We plan to investigate in detail these topics in a forthcoming paper.

We acknowledge the anonymous Referee for offering helpful suggestions. We thank D. Yong for precious information about spectroscopic observations. The present work has been supported by JINA (ND Fund #202476). Numerical calculations have been sustained by B2FH Association (<http://www.b2fh.org/>).

Element	$t_{\odot} = 9.2$ Gyr	$t_{Gal} = 13.1$ Gyr	$t_{Gal} - t_{\odot}$
Sr	69	74	5
Y	72	76	4
Zr	66	68	2
Nb	56	58	2
Mo	39	40	1
Ru	29	30	1
Rh	12	12	0
Pd	36	37	1
Ag	11	11	0
Cd	46	47	1

Table 2: The  $s$  contributions to elements from Sr to Cd at  $t_{\odot} = 9.2$  Gyr and  $t_{Gal} = 13.1$  Gyr.

## REFERENCES

- Abia, C., Domínguez, I., Gallino, R. et al. 2002, *ApJ*, 579, 817
- Anders, F., Chiappini, C., Rodrigues, T. S., et al. 2016, *A&A*, eprint arXiv:1604.07763
- Andrievsky, S. M., Spite, F., Korotin, S. A. 2011, *A&A*, 530, A105
- Argast D., Samland M., Thielemann F.-K., Qian Y.-Z., 2004, *A&A*, 416, 997
- Aoki, W., Beers, T. C., Young, S. L., et al. 2013, *ApJ*, 145, 13
- Aoki, W., & Honda, S. 2008, *PASJ*, 60, L7
- Arcones, A., & Thielemann, F.-K. 2013, *J. Phys. G: Nucl. Part. Phys.*, 40, 013201
- Arlandini, C., Käppeler, F., Wisshak, K., Gallino, R., Lugaro, M., Busso, M., & Straniero, O. 1999, *ApJ*, 525, 886
- Battistini, C., & Bensby, T. 2016, *A&A*, 586, A49
- Bensby, T., Feltzing, S., Oey, M. S., et al. 2014, *A&A*, 562, 71
- Bensby, T., Feltzing, S., & Lundström, I. 2003, *A&A*, 410, 527
- Best, A., Bears, M. Görres, J., et al. 2013, *Phys. Rev. C*, 87, 045805
- Bird, J. C., Kazantzidis, S., Weinberg, D. H., et al. 2013, *ApJ*, 773, 43
- Bisterzo, S., Travaglio, C., Gallino, R., Wiescher, M., Käppeler, F. 2014, *ApJ*, 787, 10
- Bisterzo, S., Gallino, R., Straniero, O., Cristallo, S., & Käppeler, F. 2010, *MNRAS*, 404, 1529
- Busso, M., Gallino, R., Lambert, D. L., Travaglio, C., & Smith, V. V. 2001, *ApJ*, 557, 802

- Busso M., Gallino R., Wasserburg G. J. 1999, *ARA&A*, 37, 239
- Carollo, D., Beers, T. C., Lee, Y. S., et al. 2007, *Nature*, 450, 1020
- Cescutti, G., Chiappini C., 2014, *A&A*, 565, A51
- Cescutti, G., Chiappini, C., Hirshi, R., Meynet, G., Frischknecht, U. 2013, *A&A*, 552, A51
- Cescutti G. 2008, *A&A*, 481, 691
- Cescutti G., Matteucci F., Lanfranchi G. A., McWilliam A., 2008a, *A&A*, 491, 401
- Chiappini, C., Frischknecht, U., Meynet, G., et al. 2011, *Nature*, 472, 454
- Chiappini, C., Matteucci, F., Gratton, R. 1997, *ApJ*, 477, 765
- Cohen, J., Christlieb, N., Thompson, I., et al. 2013, *ApJ*, 778, 56
- Cowan, J. J., Rose, W. K., 1977, *ApJ*, 212, 149
- Cristallo, S., Abia, C., Straniero, O., Piersanti, L. 2015, *ApJ*, 801, 53
- Cristallo, S., Piersanti, L., Straniero, O., Gallino, R., Domínguez, I., Abia, C., Di Rico, G., Quintini, M., & Bisterzo, S. 2011, *ApJS*, 197, 17
- Cristallo, S., Straniero, O., Gallino, R., Piersanti, L., Domínguez, I., & Lederer, M. T. 2009, *ApJ*, 696, 797
- Dardelet, L., et al., 2015, *Proc. Sci.*, XIII Nuclei in the Cosmos. Debrecen, Hungary
- Denissenkov, P. A., & Tout, C. A. 2003, *MNRAS*, 340, 722
- Edvardsson, B., Andersen, J., Gustafsson, B., et al. 1993, *A&A*, 275, 101
- Eichler, M., Arcones, A., Kelic, A. et al. 2015, *ApJ*, 808, 30



- Goriely, S., Bauswein, A., Just, O., Pllumbi, E., Janka, H.-Th. 2015, MNRAS, 452, 3894
- Frischknecht, U., Hirschi, R., Thielemann, F.-K. 2012, A&A, 538, L2
- Frischknecht, U., Hirschi, R., Pignatari, M., et al. 2016, MNRAS, 456, 1803
- Goriely, S., Mowlavi, N. 2000, A&A, 362, 599
- Greggio, L. 2005, A&A, 441, 1055
- Guandalini, R., & Cristallo, S. 2013, A&A, 555, 120
- Hachisu, I., Kato, M., Saio, H., Nomoto, K. 2012, ApJ, 744, 69
- Hansen, C. J., Andersen, A. C., & Christlieb, N. 2014, A&A, 568, A47
- Hansen, C. J., Montes, F., Arcones, A. 2014a, ApJ, 797, 123
- Hansen, T., Hansen, C. J., Christlieb, N., et al. 2014, ApJ, 787, 162
- Hansen, C. J., Primas, F., Hartman, H., et al. 2012, A&A, 545, A31
- Hayden, M. R., Bovy, J., Holtzman, J. A., et al. 2015, ApJ, 808, 132
- Hawkins, K., Jofrè, P., Masseron, T., Gilmore, G. 2015, MNRAS, 453, 758
- Herwig, F., Pignatari, M., Woodward, P. R., et al. 2011, ApJ, 727, 89
- Herwig, F., Blocker, T., Schönberner, D., & El Eid, M. 1997, A&A, 324, L81
- Hillebrandt, W., Kromer, M., Röpke, F. K., Ruiter, A. J. 2013, FrPhy, 8, 116 0
- Hirschi, R. 2007, A&A, 461, 571
- Ishigaki, M. N., Aoki, W., Chiba, M. 2013, ApJ, 771, 67
- Ishimaru, Y., & Wanajo, S. 1999, ApJ, 511, L33

- Jadhav M., Pignatari M., Herwig F., Zinner E., Gallino R., Huss G. R., 2013, *ApJ*, 777, 27
- Jones, S., Ritter, C., Herwig, F., Fryer, C., Pignatari, M., Bertolli, M. G., Paxton, B. 2016, *MNRAS*, 455, 3848
- Käppeler, F., Gallino, R., Bisterzo, S., & Aoki, W. 2011, *Rev. Mod. Phys.*, 83, 157
- Käppeler, F., Beer, H., Wisshak, K., Clayton, D. D., Macklin, R. L., Ward, R. A., 1982, *ApJ*, 257, 821
- Karakas, A. I., Lattanzio, J. C. 2014, *PASA*, 31, e030
- Karakas, A. I. 2010, *MNRAS*, 403, 1413
- Kratz, K-L., Farouqi, K., & Möller, P., *ApJ*, 792, 6
- Kobayashi, C., Nomoto, K., & Hachisu, I. 2015, *ApJ*, 804, L24
- Kobayashi, C., & Nakasato, N. 2011, *ApJ*, 729, 16
- Kobayashi, C., & Nomoto, K. 2009, *ApJ*, 707, 1466
- Kobayashi, C., Tsujimoto, T., Nomoto, K., Hachisu, I., Kato, M. 1998, *ApJ*, 503, L155
- Kordopatis, G., Wyse, R. F. G., Gilmore, G. et al. 2015, *A&A*, 582, A122
- Langer, N., Heger, A. Wellstein, S., & Herwig, F. 1999, *A&A*, 346, L37
- Liu, N., Savina, M. R., Gallino, R., Davis, A. M., Bisterzo, S., Gyngard, F., Käppeler, F., Cristallo, S., Dauphas, N., Pellin, M. J., Dillmann, I. 2015, *ApJ*, 803, 12
- Liu, N., Savina, M. R., Davis, A. M., et al. 2014, *ApJ*, 786, 66
- Lodders, K., Palme, H., & Gail, H.-P. 2009, *Landolt-Börnstein - Group VI Astronomy and Astrophysics Numerical Data and Functional Relationships in Science and Technology*, Edited by J.E. Trümper, 4B: solar system, 4.4

- Lugaro, M., Campbell, S. W., Van Winckel, H., et al. 2015, *A&A*, 583, A77
- Lugaro, M., Karakas, A., Stancliffe, R. J., & Rijs, C. 2012, *ApJ*, 747, 2
- Maeder, A., & Meynet, G. 2012, *Rev. Mod. Phys.*, 84, 25
- Maiorca, E., Magrini, L., Busso, M., et al. 2012, *ApJ*, 747, 53
- Maoz, D., Mannucci, F., & Nelemans, G. 2014, *ARA&A*, 52, 107
- Marquardt, k. S., Sim, S. A., Ruiter, A.J., et al. 2015, *A&A*, 580, A118
- Mashonkina, L., & Christlieb, N. 2014, *A&A*, 565, 123
- Matteucci, F., Romano, D., Arcones, A., Korobkin, O., Rosswog, S. 2014, *MNRAS*, 438, 2177
- Matteucci F., Spitoni E., Recchi S., Valiante R., 2009, *A&A*, 501, 531
- Meynet, G., Ekström, S., & Maeder, A. 2006, *A&A*, 447, 623
- Minchev, I., Martig, M., Streich, D., et al. 2015, *ApJ*, 804, L9
- Mishenina, T. V., Pignatari, M., Carraro, G., et al. 2015, *MNRAS*, 446, 3651
- Mishenina, T. V., Pignatari, M., Korotin, S. A., et al. 2013, *A&A*, 552, 128
- Montes, F., Beers, T. C., Cowan, J., et al. 2007, *ApJ*, 671, 1685
- Nishimura , N., Takiwaki, T., Thielemann, F-K. 2015, *ApJ*, 810, 109
- Nissen, P. E., & Schuster, W. J. 2011, *A&A*, 530, A15
- Nucci, M. C., Busso, M. 2014, *ApJ*, 787, 141
- Pereira, J., & Montes, F. 2016, *Phys. Rev. C*, 93, 4611

- Peterson, R. C. 2013, *ApJ*, 768, L13
- Piersanti, L., Cristallo, S., & Straniero, O. 2013, *ApJ*, 774, 98
- Pignatari, M., Hirshi, R., Wiescher, M., et al. 2013, *ApJ*, 762, 31
- Pignatari, M., Gallino, R., Heil, M., Wiescher, M., Käppeler, F., Herwig, F., & Bisterzo, S. 2010, *ApJ*, 710, 1557
- Pignatari M., Gallino R., Meynet G., Hirschi R., Herwig F., Wiescher M., 2008, *ApJ*, 687, L95
- Placco, V. M., Frebel, A., Beers, T. C., et al. 2014, *ApJ*, 781, 40
- Qian, Y.-Z., & Wasserburg, G. J. 2008, *Physics Reports*, 442, 237
- Raiteri, C. M., Gallino, R., Busso, M. 1992, *ApJ*, 387, 263
- Reddy, B. E., Tomkin, J., Lambert, D. L., Allende Prieto, C. 2003, *MNRAS*, 340, 304
- Rix, H.-W., & Bovy, J., 2013, *åR*, 21, 61
- Roederer, I. U., Karakas, A. I., Pignatari, M., Herwig, F. 2016, *ApJ*, 821, 37
- Roederer, I. U., Cowan, J. J., Preston, G. W., Sheckman, S. A., Sneden, C., Thompson, I. B. 2014, *MNRAS*, 445, 2970
- Roederer, I. U., Preston, G. W., Thompson, I. B., Sheckman, S. A., Sneden, C., Burley, G. S., Kelson, D. D. 2014a, *AJ*, 147,136
- Roederer, I. U. 2012, *ApJ*, 145, 26
- Roederer, I. U., Lawler, J. E., Sobeck, J. S., et al. 2012, *ApJS*, 203, 27
- Roederer, I. U., Cowan, J. J., Karakas, A. I., et al. 2010, *ApJ*, 724, 975

- Ruiz-Lapuente, P. 2014, *New Astron. Rev.*, 62, 15
- Ruiter A. J., Belczynski K., & Fryer C., 2009, *ApJ*, 699, 2026
- Shen, S., Cooke, R., Ramirez-Ruiz, E., Madau, P., Mayer, L., Guedes, J. 2015, *ApJ*, 807, 115
- Siess, L., Goriely, S., & Langer, N. 2004, *A&A*, 415, 1089
- Simmerer, J., Sneden, C., Cowan, J. J., Collier, J., Woolf, V. M., Lawler, J. E. 2004, *ApJ*, 617, 1091
- Siqueira Mello, Jr. C., Andrievsky, S. M., Barbuy, B., Spite, M., Spite, F., Korotin, S. A. 2015, *A&A*, 584, 86
- Siqueira Mello, Jr. C., Hill, V., Barbuy, B., et al. 2014, *A&A*, 565, 93
- Stancliffe, R. J., Dearborn, D. S. P., Lattanzio, J. C., Heap, S. A., Campbell, S. W. 2011, *ApJ*, 742, 121
- Stello, D., Huber, D., Sharma, S., et al. 2015, *ApJ*, 809, L3
- Straniero, O., Cristallo, S., & Piersanti, L. 2014, *ApJ*, 785, 77
- Straniero, O., Gallino, R., & Cristallo, S. 2006, *Nucl. Phys. A*, 777, 311
- Straniero, O., Gallino, R., Busso, M., Chieffi, A., Raiteri, C. M., Limongi, M., Salaris, M. 1995, *ApJ*, 440, 85
- Travaglio, C., Gallino, R., Rauscher, T., Röpke, f. K., Hillebrandt, W. 2015, *ApJ*, 799, 54
- Travaglio, C., Hillebrandt, W., & Reinecke, M. 2005, *A&A*, 443, 1007
- Travaglio, C., Gallino, R., Arnone, E., Cowan, J., Jordan, F., & Sneden, C. 2004, *ApJ*, 601, 864

- Travaglio, C., Gallino, R., Busso, M., & Gratton, R. 2001, *ApJ*, 549, 346
- Travaglio, C., Galli, D., Gallino, R., Busso, M., Ferrini, F., & Straniero, O. 1999, *ApJ*, 521, 691
- Trippella, O., Busso, M., Maiorca, E., Käppeler, F., Palmerini, S. 2014, *ApJ*, 787, 41
- Tur, C., Heger, A., Austin, S. M. 2009, *ApJ*, 702, 1068
- van de Voort, F., Quataert, E., Hopkins, P. F., Keres, D., Faucher-Giguère, C.-A. 2015, *MNRAS*, 447, 140
- Wehmeyer, B., Pignatari, M., & Thielemann, F.-K. 2015, *MNRAS*, 452, 1970
- Winteler, C., Käppeli, R., Perego, A., et al. 2012, *ApJ*, 750, L22
- Woodward, P. R., Herwig, F., Lin, P.-H. 2015, *ApJ*, 798, 49
- Yong, D., Norris, J. E., Bessell, M. S., et al. 2013, *ApJ*, 762, 26